Iron oxide magnetic nanoparticles with versatile surface functions based on dopamine anchors. Nanoscale

ARTICLE *in* NANOSCALE · FEBRUARY 2013

Impact Factor: 7.39 · DOI: 10.1039/c3nr33506b · Source: PubMed

Nanoscale

RSC Publishing

PAPER

View Article Online
View Journal

Iron oxide magnetic nanoparticles with versatile surface functions based on dopamine anchors

Cite this: DOI: 10.1039/c3nr33506b

Mykola Mazur,[ab] Alexandre Barras,[a] Victor Kuncser,[c] Andrei Galatanu,[c] Vladimir Zaitzev,[b] Kostiantyn V. Turcheniuk,[af] Patrice Woisel,[d] Joel Lyskawa,[d] William Laure,[d] Aloysius Siriwardena,[e] Rabah Boukherroub[a] and Sabine Szunerits*[a]

Received 6th November 2012
Accepted 2nd January 2013

DOI: 10.1039/c3nr33506b

www.rsc.org/nanoscale

The synthesis of multifunctional magnetic nanoparticles (MF-MPs) is one of the most active research areas in advanced materials as their multifunctional surfaces allow conjugation of biological and chemical molecules, thus making it possible to achieve target-specific diagnostic in parallel to therapeutics. We report here a simple strategy to integrate in a one-step reaction several reactive sites onto the particles. The preparation of MF-MPs is based on their simultaneous modification with differently functionalized dopamine derivatives using simple solution chemistry. The formed MF-MPs show comparable magnetic properties to those of naked nanoparticles with almost unaltered particle size of around 25 nm. The different termini, amine, azide and maleimide functions, enable further functionalization of MF-MPs by the grafting-on approach. Michael addition, Cu(I) catalyzed « click » chemistry and amidation reactions are performed on the MF-MPs integrating subsequently 6-(ferrocenyl)-hexanethiol, horseradish peroxidase (HRP) and mannose.

1 Introduction

Magnetic nanoparticles have demonstrated great promise for diagnostic and therapeutic applications.[1–3] Their responses to external magnetic fields allow biomolecules to be tagged and detected magnetically, enabling some exciting new approaches for bioseparation, biodetection, and targeted drug delivery. The magnetic particles should be, for these and other applications, biocompatible, hydrophilic and modified with the target agent. The attachment of desired functional groups in required quantity and with preferred orientation as well as the formation of MF-MPs remains a major challenge.[4] Surface modification of magnetic particles relies currently on mainly three approaches:[1,5–9] (i) non-covalent approaches based on adsorption of biofunctional molecules (*e.g.* antibodies, proteins, *etc*), surfactants such as oleic acid and/or oleylamine or polymers (*e.g.* polystyrene-poly acrylacid block copolymers, polyethylene glycol), (ii) coating with other semiconducting or metallic precursors producing core–shell or heterodimer structures and (iii) covalent approaches, based on the formation of relatively stable linker between hydroxyl groups on the nanoparticles surface and suitable anchoring agents such as phosphonic acid and dopamine derivatives.[6,7,10–15] A widely used robust and versatile anchor on the surface of iron oxide nanoparticles is dopamine.[13,16,17] A comprehensive review by Yuen *et al.*[17] covers the interplay of catechol ligand with iron oxide nanoparticles. The linkage is based on the chelation of the hydroxyl groups of dopamine with the surface iron atoms rendering the particles at the same time water dispersible. The amine-functions on dopamine allows for post-functionalization of the dopamine coated magnetic particles with carboxylic acid derivatives.[13,16] The group of Müller used alkyne-modified magnetic nanoparticles to attach in a Huisgen [2 + 3] cycloaddition clickable fluorescent linkers as well as azido-end group functionalized poly(ethylene glycol).[16] Dopamine based derivatives could thus represent an ideal choice for the construction of MF-MPs.

We present in this paper an easy and versatile one-step surface functionalization strategy allowing simultaneous incorporation of various functionalities onto magnetic nanoparticles. In a proof of principle we modified magnetic nanoparticles simultaneously with dopamine anchors bearing azide, maleimide and alkyne terminal groups by simple immersion of freshly prepared iron oxide nanoparticles in an anhydrous acetonitrile solution containing the respective dopamine derivatives in stoichiometric amounts. Subsequent post-synthetic multifunctional modification of the MF-MPs was performed on

[a]*Institut de Recherche Interdisciplinaire (IRI, USR 3078 CNRS), Université Lille 1, Parc de la Haute Borne, 50 Avenue de Halley, BP 70478, 59658 Villeneuve d'Ascq, France. E-mail: sabine.szunerits@iri.univ-lille1.fr; Fax: +33 3 62 53 17 01; Tel: +33 3 62 53 17 25*

[b]*Taras Shevchenko University, 60 Vladimirskaya str., Kiev, Ukraine*

[c]*National Institute of Materials Physics, Atomistilor 105 bis, 077125 Magurele, Romania*

[d]*Université Lille 1, Unité des Matériaux Et Transformations (UMET, UMR 8207 CNRS), Ingénierie des Systèmes polymères (ISP) Team, F-59655, Villeneuve d'Ascq Cedex, France*

[e]*Laboratoire des Glucides (FRE 3517 CNRS), Université de Picardie Jules Vernes, 33 rue saint Leu, 80039 Amiens, France*

[f]*Institute of Bioorganic Chemistry & Petrochemistry, National Academy of Sciences of Ukraine, 1 Murmanskaya, Kiev, Ukraine*

the different moieties: (i) the thiol functions of 6-(ferrocenyl)-hexanethiol were reacted specifically with the maleimide-arms in a Michael addition. (ii) the amine groups allowed linking of carboxyl-terminated molecules such as horseradish peroxidase (HRP) and (iii) a « click » chemistry approach was used to react the azide groups with alkynyl-terminated mannose.

2 Experimental part

2.1 Materials

All chemicals were reagent grade or higher and were used as received unless otherwise specified. Ammonium hydroxide, iron(II) chloride tetrahydrate ($FeCl_2 \cdot 4H_2O$), iron(III) chloride hexahydrate ($FeCl_3 \cdot 6H_2O$), copper(I) iodide, *N*-hydroxysuccinimide (98%, NHS), *N*-(3-dimethylaminopropyl)-*N*′-ethylcarbodiimide (98%, EDC), horseradish peroxidase (HRP, EC 1.11.1.7, type II), triethylamine (≥99.5%, TEA), sulfuric acid (95–97%), phenol (5 wt% water solution), 6-(ferrocenyl)-hexanethiol, 6-maleimidohexanoic acid *N*-hydroxysuccinimide ester, dopamine hydrochloride, hydrogen peroxide solution (30%), 2,2′-azino-bis(3-ethylbenzothiazoline-6-sulfonic acid) diammonium salt (98%, ABTS), acetonitrile, dimethyl sulfoxide (DMSO), dimethyl formamide (DMF), methanol and dichloromethane were purchased from Sigma-Aldrich.

The formation of α- propargyl mannopyranoside was achieved according to reports by Roy *et al.*[18] and Yeoh *et al.*[19] Azide-terminated dopamine (dopamine-N_3) was synthesized as reported in ref. 20.

2.2 Synthesis of maleimide-terminated dopamine

Dopamine hydrochloride (1.92 g, 0.010 mol) and 1.28 g of triethylamine (0.013 mol) dissolved in anhydrous methanol (10 mL) were added dropwise to a solution of 6-maleimidohexanoic acid *N*-hydroxysuccinimide ester (2.6 g, 0.008 mol) in anhydrous CH_2Cl_2 (100 mL). The reaction was stirred vigorously for 48 h under nitrogen. The solvents were evaporated under reduced pressure, and the residue was dissolved in dichloromethane (100 mL). The organic phase was washed three times with HCl (0.5 M, 80 mL) and dried over $MgSO_4$. After filtration, the solvent was evaporated and the crude product was purified by column chromatography (SiO_2/CH_2Cl_2/MeOH 10:1). The product was obtained as a yellow solid in 30% yield. ^{1}H NMR (300 MHz, $CDCl_3$): 1.22 (m, 2H, CH_2–*CH_2*–CH_2), 1.55 (m, 4H, N–CH_2–*CH_2* and *CH_2*–CH_2–CO–NH), 2.12 (t, 2H, *CH_2*–CO–NH), 2.66 (t, 2H, *CH_2*–Ar), 3.44–3.46 (m, 4H, N–*CH_2*–CH_2, *CH_2*–NH–CO), 5.94 (t, 1H, *NH*–CH_2), 6.52 (dd, 1H, ArH), 6.66 (s, 2H, *CH*=*CH*), 6.71 (d, 1H, ArH), 6.78 (d, 1H, ArH); ^{13}C NMR (75 MHz, $CDCl_3$): 173.9 (*CO*–NH); 171.1 (*CO*–N–*CO*); 144.3, 143.1, 130.6, 120.4, 115.6, 115.3 (*CH* Ar); 134.1 (*CH*=*CH*); 40.9 (*CH_2*–N); 37.6 (*CH_2*–NH); 36.4 (*CH_2*–CO–NH); 34.8 (*CH_2*–Ar); 28.2 (N–CH_2–*CH_2*); 26.1 (CH_2–*CH_2*–CH_2); 25.1 (*CH_2*–CH_2–CO–NH).

2.3 Preparation of magnetic particles

In a typical procedure, $FeCl_2 \cdot 4H_2O$ (0.34 g, 1.7 mmol) and $FeCl_3 \cdot 6H_2O$ (0.95 g, 3.5 mmol) were dissolved in deareated water (20 mL) and subsequently added to a nitrogen-protected three-necked flask under sonication. The resulting mixture was heated at 50 °C for 30 min. Then concentrated ammonium hydroxide (2 mL) was added dropwise and kept at constant temperature (50 °C) for 30 min. The system was finally cooled to room temperature and the solid product was isolated *via* a non-uniform magnetic field generated by a Nd–Fe–B permanent magnet. The resulting Fe_3O_4 particles were washed six times with Milli-Q water to remove unreacted chemicals and then stored in water.

2.4 Preparation of dopamine modified magnetic particles

2.4.1 Modification with one dopamine derivative. 1 mL of an acetonitrile solution of either dopamine (2×10^{-2} M) or dopamine derivative (2×10^{-2} M) bearing an azide (dopamine-N_3) or a maleimide function (dopamine-MA) was added to a 2 mL suspension of Fe_3O_4 nanoparticles (30 mg mL^{-1}) in acetonitrile (Fig. 1). The dispersion was sonicated for 30 min and then washed four times with acetonitrile through consecutive washing/centrifugation cycles at 10 000 rpm.

2.4.2 Simultaneous modification with three dopamine derivatives. Fe_3O_4 nanoparticles (30 mg) dispersed in 1 mL anhydrous CH_3CN were mixed with dopamine (1.2×10^{-5} M), dopamine-N_3 (1.2×10^{-5} M) and dopamine-MA (1.2×10^{-5} M) and sonicated for 30 min and then washed four times with acetonitrile through consecutive washing/centrifugation cycles at 10 000 rpm.

2.5 Subsequent reactions of MF-MPs

2.5.1 Formation of particle MF-MP1: linking of 6-(ferrocenyl)-hexanethiol. To 100 μL of MF-MPs (10 mg mL^{-1}) dispersed in water were added 900 μL of a solution of 6-(ferrocenyl)-hexanethiol) in water/ethanol (2/2) (11 mg mL^{-1}) and stirred overnight at room temperature. The particles were then washed with PBS-tween (0.1%) for 5 min and repeatedly rinsed with water to remove any nonspecifically adsorbed reactants. The particles were stored in PBS buffer at 4 °C before use.

2.5.2 Formation of particle MF-MP2: horseradish peroxidase immobilization. HRP attachment onto MF-MP2 was achieved by immersion of MF-MP1 particles (10 mg mL^{-1}) in a 100 μg L^{-1} HRP solution in PBS buffer (pH 7.4) containing NHS (0.1 M) and EDC (2 mM) for 24 h at room temperature. The particles were then washed with PBS-tween (0.1%) for 5 min and repeatedly rinsed with water to remove any nonspecifically adsorbed enzyme. The particles were stored in PBS buffer at 4 °C before use.

2.5.3 Formation of particle MF-MP3: "clicking" α-propargyl mannopyranoside to the azide function. The linking of α-propargyl mannopyranoside to azide function on MF-MP2 particles was achieved by addition of α-propargyl mannopyranoside (1 mM), CuI (3.15 mM) and TEA (43 mM) to a suspension of MF-MP2 (10 mg) in anhydrous acetonitrile (10 mL) and subsequent stirring for 24 h at room temperature. The resulting nanoparticles were separated by magnetic force and purified through consecutive wash/centrifugation cycles at 10 000 rpm with acetonitrile (twice).

2.6 Assay for the detection of hydrogen peroxide on MF-MP3

A classical colorimetric reaction was used to explore the presence of HRP on MF-MP3 particles. MF-MP3 particles (0.5 mg mL^{-1}) were immersed into a UV/vis cuvette containing 3.6 mM of 2,2′-azino-bis-(3-ethylbenzothiazoline-6-sufonic acid)

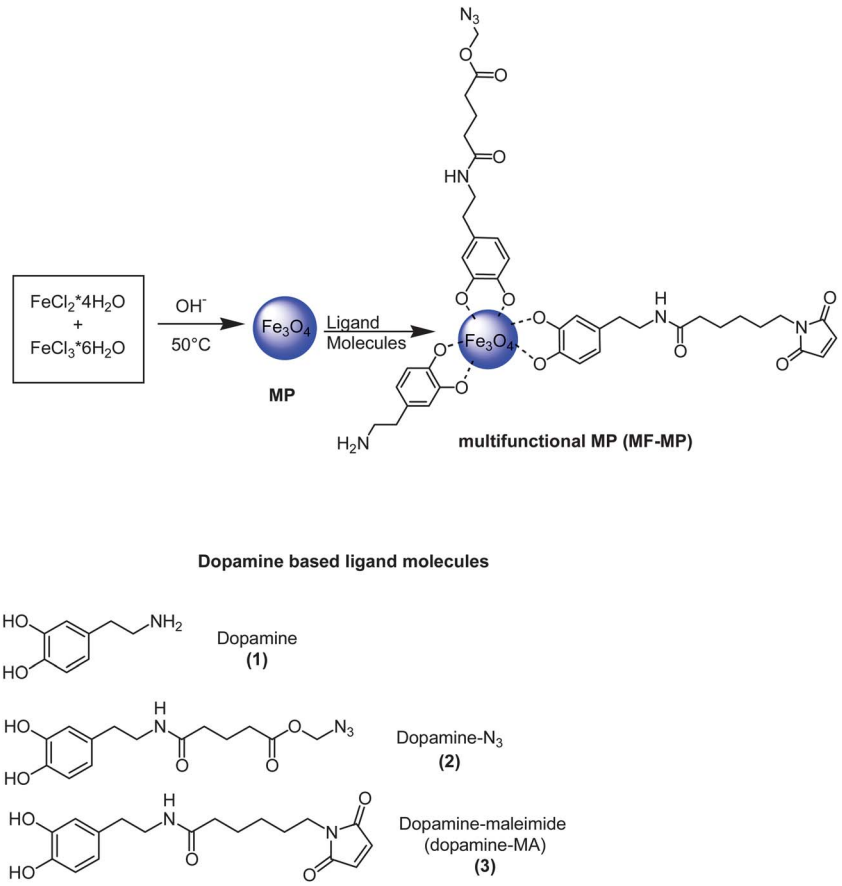

Fig. 1 Schematic illustration of the formation of MF-MPs based on the use of differently functionalized dopamine derivatives.

diammonium salt (ABTS) and H_2O_2 (50 μM) in PBS (2 mL). After 20 min reaction, the magnetic nanoparticles were removed and a UV/vis spectrum was recorded.

2.7 Determination of the coupling efficiency of "clicked" glycans to MF-MP3 particles

A standard calibration curve was generated for the determination of carbohydrate concentrations by mixing aliquots of aqueous phenolic solution (5 wt%, 60 μL) and concentrated H_2SO_4 (900 μL) to a series of 60 μL aliquots of serially diluted aqueous mannose solutions. Each was stirred for 10 min and then its absorption spectrum was recorded (Perkin Elmer *Lambda 950 dual beam)* using as a blank a phenol-H_2SO_4 mixture containing only 60 μL of water. The absorbance of the solution was measured at two wavelengths: $\lambda_1 = 495$ (absorption band of mannose complex) and $\lambda_2 = 570$ nm (background) and the absorbance difference (A_{495}–A_{570}) was plotted against the concentration of the corresponding carbohydrate. For determining the coupling efficiency of mannose to the MF-MP, 0.2 mg mL^{-1} of MF-MP3 were immersed for 60 min into 1 mL H_2SO_4 and 60 μL phenol and the UV/Vis spectrum was recorded.

2.8 Sample characterization

X-ray photoelectron spectroscopy. X-ray photoelectron spectroscopy (XPS) measurements were performed with an ESCALAB 220 XL spectrometer from Vacuum Generators featuring a monochromatic Al Kα X-ray source (1486.6 eV) and a spherical energy analyzer operated in the CAE (constant analyzer energy) mode (CAE = 100 eV for survey spectra and CAE = 40 eV for high-resolution spectra), using the electromagnetic lens mode. The surface was prepared by depositing 100 μL of the particle suspension (1 mg mL^{-1}) in water onto silicon wafers and let to dry. The detection angle of the photoelectrons is 30°, as referenced to the sample surface. The XPS spectra were corrected according to the binding energies of Au 4f7/2, equal to 80.0 eV.

FTIR spectroscopy. Fourier transform infrared (FTIR) spectra modes were recorded using a ThermoScientific FTIR instrument (Nicolet 8700) with a resolution of 4 cm^{-1}. Dried magnetic nanoparticles (1 mg) were mixed with KBr powder (100 mg) in an agate mortar. The mixture was pressed into a pellet under 10 tons load for 2–4 min, and the spectrum was recorded immediately. Sixteen accumulative scans were collected. The signal from a pure KBr pellet was subtracted as the background.

UV/vis measurements. Absorption spectra were recorded using a Perkin Elmer Lambda UV/Vis 950 spectrophotometer in plastic cuvettes with an optical path of 10 mm. The wavelength range was 400–1100 nm or 400–700 nm.

Magnetic measurements. Temperature and field dependent magnetic measurements have been performed by SQUID magnetometry (MPMS XL magnetometer from Quantum Design) under the high sensitivity reciprocal space option, RSO.

In addition, the Fe phase composition and local magnetic interactions were analyzed by the powerful method of the ^{57}Fe Mössbauer spectroscopy. Mössbauer spectra were collected at different temperatures between 5 K and 240 K, in transmission geometry, by inserting the sample into a close cycle He cryostat. A Mössbauer drive system operating in constant acceleration mode combined with conventional electronics and a Co(Rh matrix) source of about 30 mCi activity were employed.

Transmission electron microscopy (TEM). High resolution Transmission electron microscopy (HRTEM) images were taken by using Icon analytical 300 KeV microscope.

Particle size and zeta potential measurements. Particle suspensions (20 μg.mL^{-1}) in water were sonicated for 30 min. Then the particle size of the MF-MP suspensions was measured at 20 °C with an equilibration time of 2 min using a ZetasizerNanoZS (Malvern Instruments S.A., Worcestershire, U.K.) in 173° scattering geometry.

3 Results and discussion

3.1 Modification and characterization of iron oxide nanoparticles with dopamine derivatives

The synthesis of Fe_3O_4 nanoparticles functionalized with different dopamine-based ligands was performed in a two step process (Fig. 1). It involves the preparation of Fe_3O_4 nanoparticles by precipitation from an alkaline solution containing a mixture of iron salts (Fe^{2+}, Fe^{3+}) according to a modified procedure reported by Kang *et al.*,[21] followed by grafting three different dopamine anchors simultaneously to the magnetic particles, forming MF-MPs.[13] It is widely accepted that bidentate enediol ligands such as dopamine and its derivatives convert the under-coordinated Fe surface sites back to a bulk-like lattice structures with an octahedral geometry for oxygen-coordinated ion, being the cause of the tight binding of dopamine-ligands to iron oxide.[22] The size of the magnetic particles before and after modification with the dopamine capping ligands was investigated by transmission electron microscopy (Fig. 2). The TEM images of Fe_3O_4 nanoparticles (Fig. 2A) and of the MF-MPs (Fig. 2B) reveal a size distribution in the range of 25 ± 1.5 nm (Fig. 2C) for both particles.

A detailed characterization of the surface composition of the as-synthesized Fe_3O_4 nanocrystals before and after modification with dopamine derivatives was obtained by XPS (Fig. 3). The XPS survey spectrum of as-synthesized Fe_3O_4 nanoparticles shows strong bands due to iron at 724 eV ($Fe2p_{1/2}$), 709 eV ($Fe2p_{3/2}$) and 60 eV (Fe3p), and oxygen at 515 eV (O1s) (Fig. 3Aa). The presence of a small band at 285 eV (≈7 at.%) is most likely due to carbon impurities adsorbed on the particles. The Fe/O ratio is 0.73, being somewhere in-between that of Fe_3O_4 (0.75) and Fe_2O_3 (0.66), indicating that some magnetic Fe_3O_4 got oxidized into Fe_2O_3. Indeed, the high resolution Fe2p core level spectrum shows next to the narrow and strong band at 709.5 eV ($Fe2p_{3/2}$) and the weaker band at 722.6 eV ($Fe2p_{1/2}$), additional satellite peaks: one being located approximately 8 eV higher than the main $Fe2p_{3/2}$ peak, the other 8.4 eV higher than the weaker band $Fe2p_{1/2}$ (Fig. 3B). The peak position and the presence of the satellite peaks are typical of Fe_2O_3.[23]

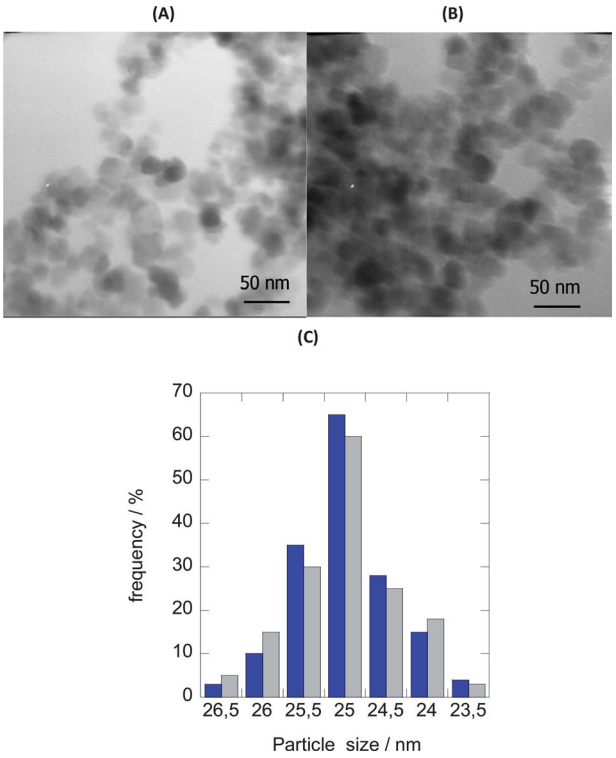

Fig. 2 TEM images of Fe_3O_4 nanocrystals (A) and of MF-MPs (B); Size distribution of Fe_3O_4 nanocrystals (grey) and MF-MPs (blue).

XPS survey spectra of Fe_3O_4 nanoparticles functionalized with each dopamine anchor (*i.e.* dopamine, dopamine-N_3 or dopamine-MA) (Fig. 1) and simultaneously with these 3 dopamine derivatives are displayed in Fig. 3Ab–e. In all cases, in addition to bands due to C1s, O1s and iron ($Fe2p_{3/2}$, Fe3p, $Fe2p_{1/2}$) of the magnetic particles, a band around ≈400 eV due to N1s is seen, suggesting the presence of dopamine ligands on the particles surface. Table 1 summarizes the atomic percentage of the individual elements. The use of the ratio of C/N for dopamine (theoretical: 7.0, experimental: 6.7), dopamine-N_3 (theoretical: 3.0, experimental: 5.1) and dopamine-MA (theoretical: 6.0, experimental: 7.6) is a good estimation for the success of the surface reaction. In the case of dopamine, the experimental value matches well the theoretical one, while in the other two cases the carbon content is somewhat higher. The high values of C/N ratios for Fe_3O_4 modified with dopamine-N_3 and dopamine-MA are most likely due to some carbon impurities. The MF-MPs show an experimental C/N ratio of 6.7 (theoretical 5.7) being somewhat higher than expected. The atomic percentage of N1s is in-between that of magnetic particles modified with dopamine-N_3 and dopamine-MA and indicates full coverage of the magnetic particles with the three dopamine ligands.

The signature of the different nitrogen contributions in the high resolution of the N1s core level spectrum was investigated in more details (Fig. 4). For comparison, the deconvoluted N1s spectra of Fe_3O_4 modified with only one of the dopamine-derivatives was included. In the case of dopamine modified particles the N1s spectrum could be deconvoluted into two

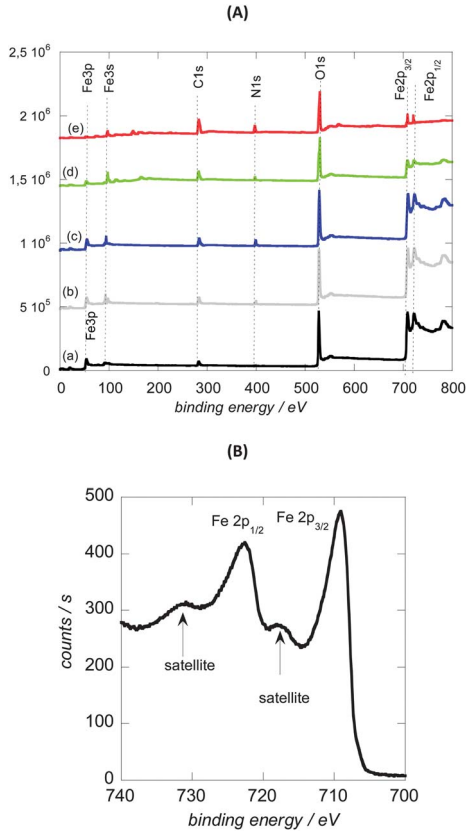

Fig. 3 (A) XPS survey spectra of as prepared magnetic particles before (a, black) and after modification with dopamine (b, grey), dopamine-N_3 (c, blue), dopamine-MA (d, green) and of MF- MP (e, red). (B) High resolution Fe2p spectrum of as-synthesized magnetic particles.

components at 398.4 eV (NH_2) and 400.43 (NH_3^+) in a 1/1 ratio (Fig. 4a). The presence of a certain amount of protonated amine groups is in agreement with the observed positive zeta potential of $\zeta = 14 \pm 3$ mV. In the case of dopamine-N_3 modified particles, the presence of the $-N_3$ function is unambiguously revealed by the bands at 404.5 (N=N^+=N^-) and 400.9 eV (N=N^+=N^-), characteristic to the azide group (Fig. 4b). In addition, a band at 399.8 eV due to O=C–N– is observed with a ratio of 1/2/1 N=N^+=N^-/N=N^+=N^-/O=C–N– as theoretically expected. In the case of dopmaine-MA functionalized particles, a band at 399.8 eV was observed in accordance with the presence of O=C–N– functional groups (Fig. 4c). As seen in Fig. 4d, the simultaneous reaction of the three dopamine ligands with Fe_3O_4 particles results in XPS signature of the N1s band

Table 1 Atomic percentage of magnetic particles modified with different dopamine ligands

Particles modified with	C1s (at.%)	O1s (at.%)	N1s (at.%)	Fe2p (at.%)
Dopamine (1)	7.51	54.02	1.11	37.36
Dopamine-N_3 (2)	17.87	57.37	3.53	21.23
Dopamine-maleimide (3)	19.65	56.54	2.58	21.23
1 + 2 + 3	15.95	58.89	2.39	22.77
Naked particles	4.94	54.95	0.00	40.11

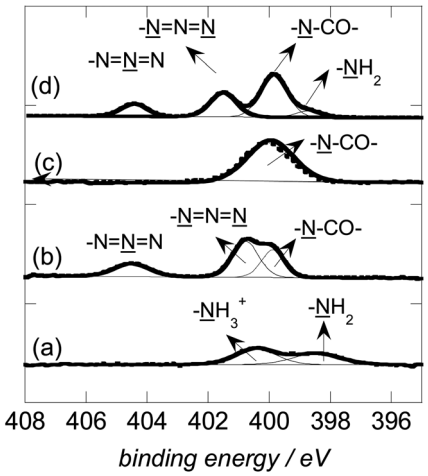

Fig. 4 XPS N1s high resolution spectrum of magnetic particles modified with dopamine (a), dopamine-N_3 (b), dopamine-MA (c) and MF-MPs (d).

comprising all the previous ones: 404.5 (N=N^+=N^-), 401.6 eV (N=N^+=N^-), 399.9 eV (O=C–N– and some –NH_3^+) and 398.8 eV (–NH_2) with a ratio of 1 : 1.9 : 3.4 : 0.5 close to theoretical predicted values (1 : 2 : 3 : 1). In that case, some of the –NH_2 groups are protonated which correlates with the lower amount found for the 398.8 eV band and a higher amount obtained for the 399.9 eV peak.

The XPS results are corroborated by the FT IR analysis in Fig. 5. The FTIR spectrum of the as-prepared Fe_3O_4 particles displays a broad band centered at 3423 cm^{-1} assigned to the vibration of the hydroxyl groups and/or adsorbed water molecules on the surface of the particles. The strong band at 1629 cm^{-1} is due to OH deformation modes of the hydroxyl groups and adsorbed water.[24,25] The FTIR spectrum of the dopamine-modified magnetic particles exhibits additional bands consistent with the main vibration modes of dopamine such as the C–H vibration at 2927 cm^{-1}, the NH stretching at 3367 cm^{-1} and the NH bending vibration of primary amine at 1619 cm^{-1}.[22,25] The intense C–O stretching of the phenolic OH is located at 1275 cm^{-1}. The C=C ring stretching band overlaps with the CH_2 scissoring band is seen at 1499 cm^{-1}. In the case of dopamine-N_3 functionalized Fe_3O_4 particles, the presence of the bands at 2108 cm^{-1}, 1725 cm^{-1} and 2940 cm^{-1} characteristic of $\nu_{as}(N_3)$, ν(C=O ester) stretching modes and C–H vibration mode is a clear evidence of the success modification of the particles with dopamine-N_3. FTIR spectrum of DOPA-MA modified Fe_3O_4 particles shows a strong band at 1725 cm^{-1} due to $\nu_{C=O}$ in accordance with the chemical composition of the particles. The MF-MPs show as in the case of XPS analysis all the characteristic bands of the individual dopamine derivatives, notably the N_3 stretching mode at 2108 cm^{-1}, $\nu_{C=O}$ of the maleimide function at 1725 cm^{-1} and the NH bending vibration of the primary amine at 1619 cm^{-1}.

3.2 Magnetic properties of iron oxide and MF-MP nanoparticles

Zero-field cooled (ZFC) and field-cooled (FC) curves were measured in a magnetic field of 80 Oe in the temperature range

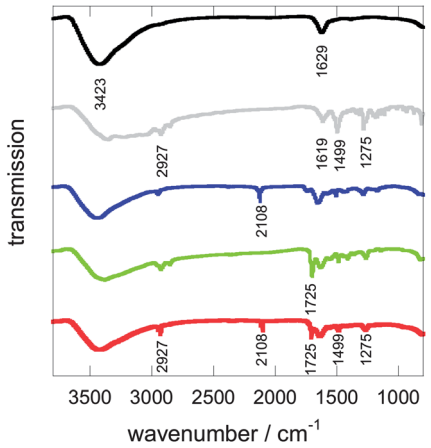

Fig. 5 FTIR spectra of magnetic particles before (black), and after modification with dopamine (grey), dopamine-N_3 (blue), dopamine-MA (green) and MF-MPs (red).

of 5–380 K, on the naked magnetic nanoparticles (Fig. 6A) as well as on those modified with three dopamine-derivatives (Fig. 6B). The ZFC and FC curves are typical for systems of magnetic monodomain nanoparticles presenting superparamagnetic behavior above a temperature which is called the blocking temperature T_B. In the present case, the two curves show a divergence point very close to the maximum of the ZFC curve, suggesting both very weak interparticle magnetic interactions as well as a very narrow size distribution of the nanoparticles in the samples.[26] On the other hand, the blocking temperature, T_B, as estimated from the maximum of the ZFC curve is lower in the case of naked magnetic particles (about 315 K) as compared to the case of the modified MF-MPs (about 350 K). Keeping in mind that the blocking temperature, defined as a parameter which is dependent on the time window of the measuring method, is proportional to the anisotropy energy of the nanoparticle, KV, with K the anisotropy constant and V the volume of the nanoparticle,[27] it results directly that the anisotropy energy of modified nanoparticles is some 10% larger than of naked nanoparticles.

The hysteresis loops for both types of particles are also shown in Fig. 6A and B. The magnetization at saturation, as estimated by the law of approach,[22] is $\approx$84 emu/g for naked Fe_3O_4 particles[28] and 80 emu/g for dopamine derivatives modified nanoparticles. The value for naked Fe_3O_4 particles is close to the theoretical value of the spontaneous magnetization of magnetite, Fe_3O_4, corresponding to a magnetic moment of 4 μ_B per formula unit. The slightly lower value of dopamine derivatives modified nanoparticles might be explained either by a more defected magnetic structure compared to the naked magnetic particles or by a diminished relative weight of the magnetic material in the sample. A rough estimation of the number of additional non-magnetic atoms (C, O, N, except the lightest H) which might be found at the surface of a magnetite nanoparticle of 25 nm average size *via* the functionalization with the three capping ligands, in the hypothesis of newly formed Fe–O bonds satisfying all the Fe ions at the particle surface, leads to a value of about 10^6 lighter atoms. On the other hand, this magnetic particle will contain about 7×10^6 heavier atoms of Fe and oxygen. Accordingly, a value of about 0.06 can be estimated for the ratio between the weight of the shell surfactant and the core magnetite. Hence, the relative decrease of just 5% of the magnetization at saturation for the MF-MPs with respect to the naked MPs can be simply explained by the diminished weight of the magnetic material in the first sample, in conditions of negligible changes of the magnetic

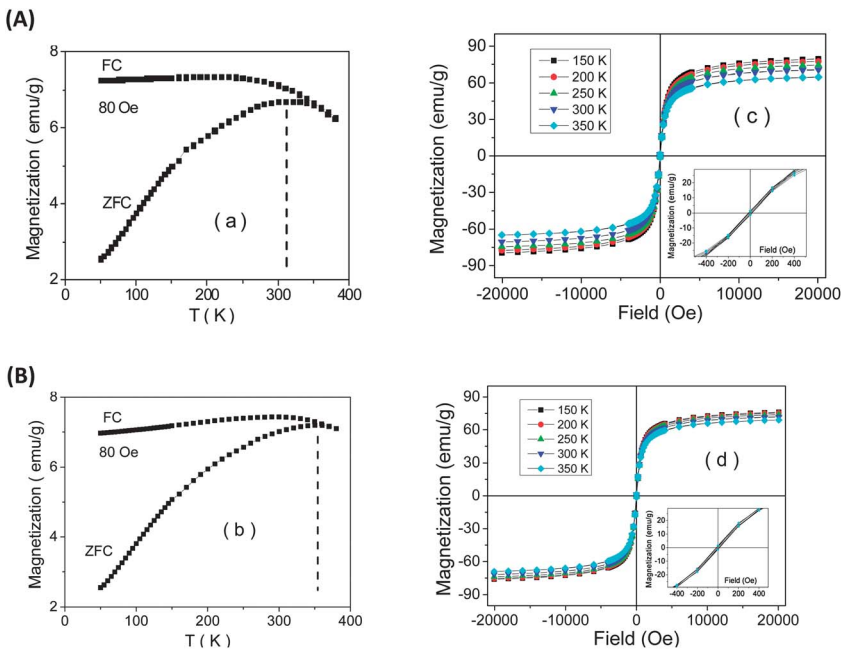

Fig. 6 ZFC-FC magnetization curves (left hand images) and temperature dependent hysteresis loops (right hand images) for (A) naked MPs and (B) MF-MPs. Insets show more resolute loops with respect to the field range, in order to better evidence the very low values of the coercive fields.

structure of the two types of nanoparticles. Interestingly, a similar estimation of the relative atomic content for the different elements, leads to values approaching the ones reported in Table 1 *via* XPS measurements on MF-MPs and naked MPs systems, only if the XPS signal comes in average from less than 2 nm from the nanoparticle surface.

The surprisingly low value of the coercive field (about 15 Oe for naked magnetic particles and 20 Oe for MF-MPs at 150 K), indicates clearly a very low anisotropy constant, as compared to the theoretical expectation of about 12 000 J m^{-3} for the bulk magnetite-like structure.[27,28] Taking into account the decreasing rate of the coercive field *versus* temperature, coercive fields of about 20 Oe and 25 Oe are reasonably estimated for the static regime at very low temperatures, for both systems respectively. While such nanoparticles are magnetic monodomains, they can be treated in the frame of the Stoner–Wohlfarth model of randomly distributed easy axis of magnetization, where the anisotropy constant can be satisfactorily approximated by the product between the coercive field and the saturation magnetization at low temperatures (in the magnetic static regime). It is easy to estimate with the above mentioned values, anisotropy constants of about 700 J m^{-3} for naked MP and 800 J m^{-3} for MF-MPs, both values being more than one order of magnitude lower than the specific value of the anisotropy constant in bulk magnetite.

The phase composition, local structure and magnetic interactions, as well as the magnetic relaxation phenomena in the two samples have been also studied *via* ^{57}Fe Mössbauer spectroscopy. Mössbauer spectra collected at different temperatures on naked magnetic particles as well as on dopamine derivatives modified magnetic nanoparticles are shown in Fig. 7A and B. All the spectra consist of broad sextets, with a line-width which is increasing *versus* temperature, as an indication of magnetic relaxation phenomena specific to fine nanoparticles in the regime of collective excitations.[29] The Mössbauer spectrum specific to bulk magnetite well above the Verwey temperature (consisting of two distinct sextets attributed to Fe ions on tetrahedral and respectively octahedral positions)[30] is not evidenced, the actual shape reminding rather that of an iron oxide nanoparticle specific structure, consisting of a gradient-like transition from an inner shell magnetite to an outer shell maghemite. Therefore, even the spectra collected at the lowest temperature of 5 K (in the magnetic static regime), could be successfully fitted by distribution of magnetic hyperfine fields corresponding to Fe ions in distributed local configurations (the powerful NORMOS program with options for both discrete and continuously distributed hyperfine parameters have been used in this respect).[31] The corresponding hyperfine field distribution probability is presented on the right of each spectrum and further Mössbauer data has been interpreted in terms of specific parameters, related to such a distribution (*e.g.* average magnetic hyperfine field, $\langle B_{hf}\rangle$, or standard deviation related to the width, ΔB_{hf}, of the distribution). Besides this broad Mössbauer sextet component, of average magnetic hyperfine field of 51.5 T and average isomer shift of 0.5 mm s^{-1} at 5 K, assigned to the distributed Fe positions in the Fe oxide mixture (gradient-like structure of Fe_3O_4–Fe_2O_3), a second weak sextet component of less than 5% spectral area has to be considered for an improved least square test. By its specific hyperfine parameters (magnetic hyperfine field of about 48 T, quadrupole correction of about −0.2 mm s^{-1} and isomer shift of about 0.9 mm s^{-1}), this component can be assigned to either an additional very defective Fe oxide as an impurity or more probably to very defective Fe positions located on the particle surface. While this component appears with the same insignificant relative spectral area in the Mössbauer spectra of both naked MPs and MF-MPs particles up to temperatures of 250 K, it will not be considered as defining the difference between local Fe configurations in the two systems and will be therefore neglected in the further discussion. On the other hand, concerning the width of the hyperfine field distribution, ΔB_{hf}, at low temperature, this is slightly larger for MF-MPs (6.3 ± 0.2 T) as compared to naked particles (5.6 ± 0.2 T), evidencing more distorted Fe positions induced by the dopamine coating. At increasing temperatures, the average hyperfine field decreases whereas the distribution width increases. The temperature dependencies of the reduced average magnetic hyperfine field, $\langle B_{hf}\rangle/\langle B_0\rangle$, and of the reduced distribution width $\Delta B_{hf}/\langle B_0\rangle$, with $\langle B_0\rangle$ the average hyperfine field at 5 K, are shown in Fig. 7C and D, respectively. Such linear-like dependencies are specific to magnetic relaxation phenomena in regime of collective excitations and can provide useful information about the magnetic anisotropy energy of the nanoparticles, *KV*, as well as on their relative size dispersion, $\delta D/\langle D\rangle$, with $\langle D\rangle$ the average diameter and δD the size distribution width.[27] Accordingly, the anisotropy energy may be expressed as $KV = -k_B/2SL_1$, whereas $\delta D/\langle D\rangle = -SL_2/3SL_1$ (k_B is the Boltzmann constant, SL_1 is the slope of the linear decrease of the relative average hyperfine field *versus* temperature and SL_2 is the slope of the linear increase of the relative distribution width *versus* temperature). By using the slopes SL_1 and SL_2, as determined from Fig. 7C and D, respectively, anisotropy energies of about 1.3 × 10^{-20} J and 1.4 × 10^{-20} J have been obtained for naked and modified Fe_3O_4 particles as well as relative size dispersions of 6% and 5%, for naked and MF-MPs, respectively. With the above mentioned values for the anisotropy energy and the anisotropy constants deduced from the magnetic measurements, an average magnetic size of the nanoparticles of about 26 nm and similar for both naked and modified ones is deduced, being in good agreement with TEM data (Fig. 2). On the other hand, the relative size dispersion is slightly better in the dopamine derivatives modified particles, in conditions of similar average size, proving a beneficial role of the dopamine coating along the separation procedure.

The comparable magnetization values obtained with naked MPs and MF-MPs indicate *a priori* that the dopamine derivatives are attached mainly by physical bonds to the magnetite particles. The stability of this bond will thus dictate the potential use of these MF-MPs as well as the possibility for post-functionalization strategies. Immersion of the MF-MPs for 24 h into different organic solvents (DMSO, DMF, PBS, acetonitrile, methanol, dichloromethane) did not influence the dopamine linkage. The bond was stable by heating the MF-MPs in water up to 80 °C. Above this temperature the coating slowly decomposed.

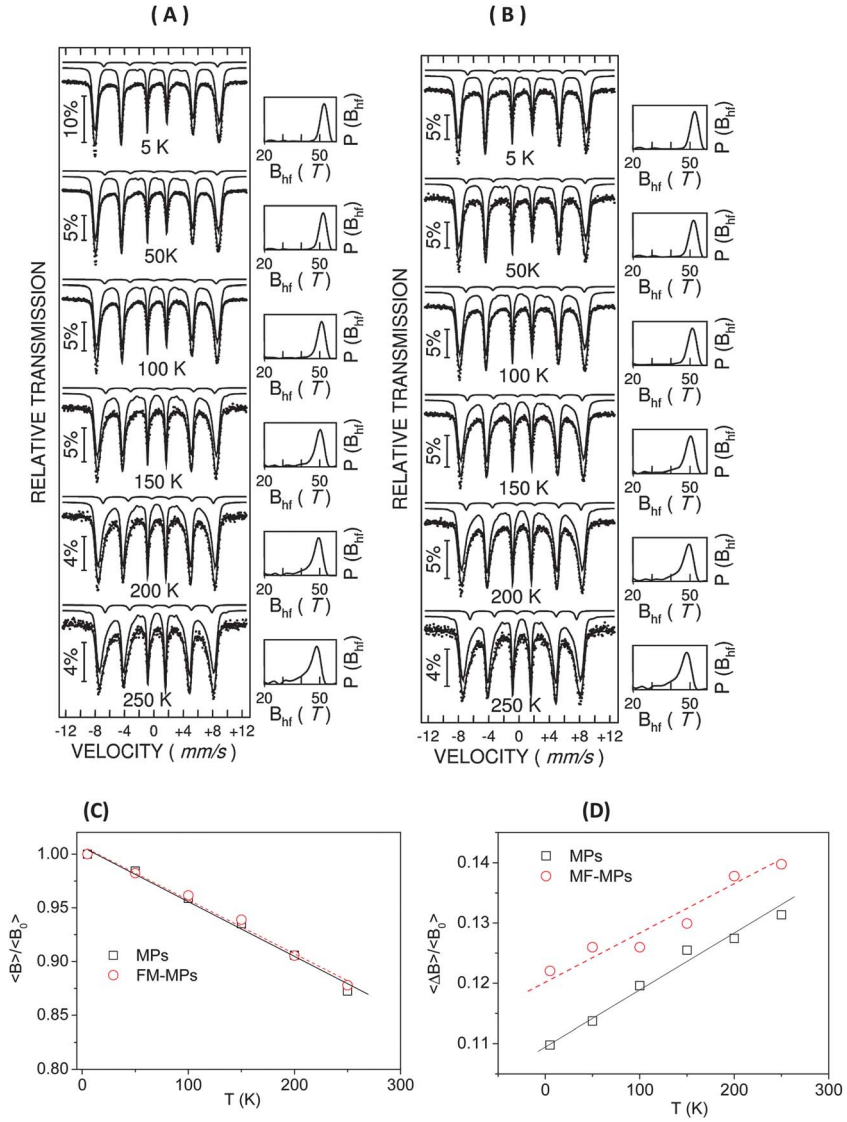

Fig. 7 Temperature dependent Mössbauer spectra of naked MPs (A) and MF-MPs, (B) as well as the temperature dependence of the reduced average magnetic hyperfine field (C) and of the reduced width of the main lobe in the hyperfine filed distribution (D), as presented on the right side of the Mössbauer spectra.

3.3 Subsequent post-functionalization strategies of MF-MPs

Usually, for a particular application, multiple surface-modification steps on the nanoparticles are required to reach the final product. Therefore, to be functional in different biomedical applications, these nanoparticles need to sustain a secondary reaction to introduce new functionalities onto their surfaces without consuming the magnetic properties of the nanoparticles. In a proof of principle study and motivated by the possibility of quantification of the linked molecules we followed the post-functionalization strategy as outlined in Fig. 8. The MF-NPs were first modified with 6-(ferrocenyl)-hexanethiol forming particles notified as MF-MP1, followed by horseradish peroxidase (HRP) (MF-MP2) and finally with propargyl-mannose (MF-MP3).

6-(Ferrocenyl)-hexanethiol was attached to MF-MPs particles through reaction of the maleimide group with the thiol groups of ferrocene (Fig. 8, reaction 1). The reaction between thiols and maleimides is commonly applied in the field of bioconjugation and thus maintains the acceptability of the process of biological applications.[32–34] In this reaction, the thiol is added across the double bond of the maleimide to yield a thioether.[33] The choice of linking 6-(ferrocenyl)-hexanethiol to the MF-MPs was motivated by the possibility of monitoring by UV/Vis spectroscopy the success of the reaction. Fig. 9A shows the UV/Vis spectrum of MF-MP1 particles (Fig. 8). The presence of ferrocene is indicated by the absorbance band at 522 nm, which corresponds to a ferrocene loading of *ca.* 20 μg mg^{-1}.

As amine-functional groups provide an obvious opportunity for the incorporation of molecules bearing COOH groups, the reactivity towards the carboxylic acid groups of horseradish peroxidase (HRP), an α-helical protein of 44 kDa, which binds heme as co-factor, was investigated (Fig. 8, reaction 2). The reaction is a one step protocol involving EDC and NHS to activate the carboxyl groups of HRP followed by direct conjugation to the iron oxide particles. The interest in linking HRP is based

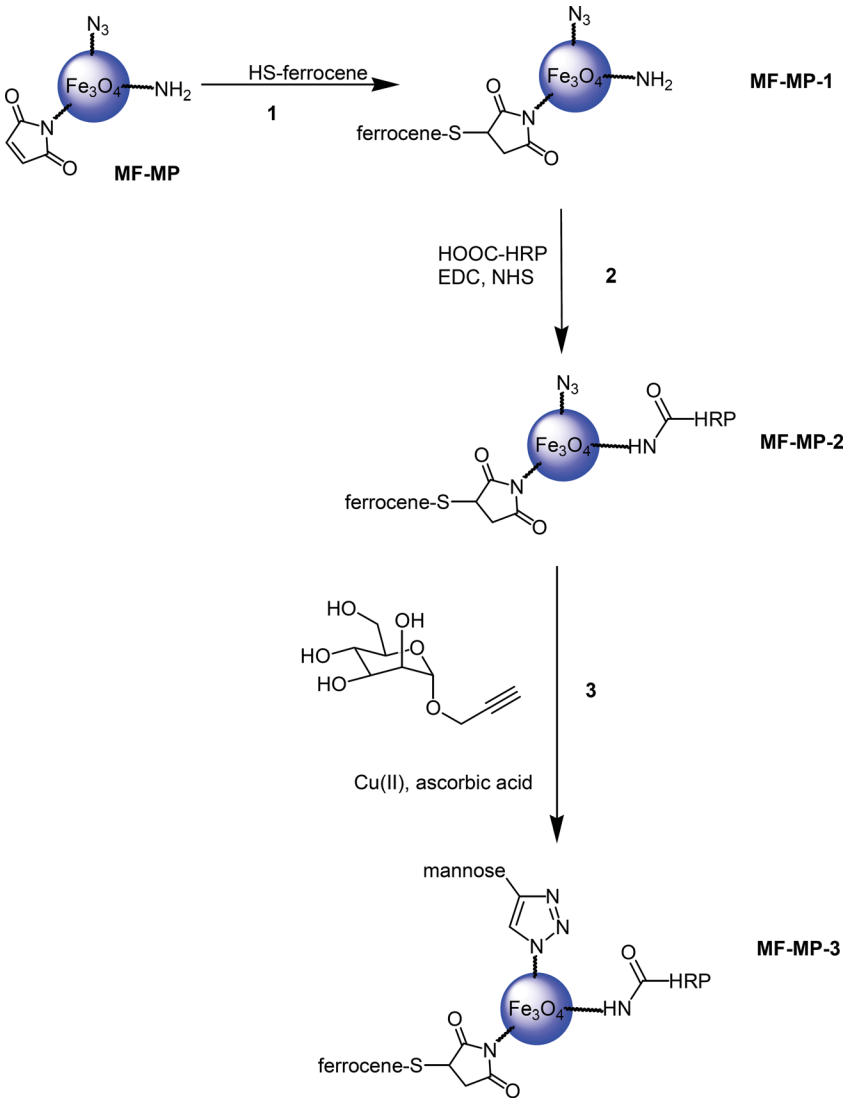

Fig. 8 Strategies for subsequent reaction possibilities; (1) Reaction of maleimide function with 6-(ferrocenyl)-hexanethiol; (2) Amidation between the amine groups of dopamine and the carboxylic acid groups of HRP, (3) "Click" reaction between azido group and alkynyl-terminated mannose in the presence of $CuSO_4$ and ascorbic acid.

on the fact that in the presence of HRP substrate such as 2′-azino-bis-(3-ethylbenzothiazoline-6-sulfonic acid) (ABTS) a colored derivative is formed, thus allowing for the quantification of covalently linked HRP using a simple spectroscopic assay as described in some other papers.[35,36] In short, it is based on the oxidation of a peroxidase substrate such as ABTS in the presence of hydrogen peroxide producing a green colored product that can be detected by spectrophotometry. Fig. 9B shows the UV/Vis spectrum of MF-MP2 after immersion into ABTS (3.6 mM) and H_2O_2 (50 μM) in PBS for 30 min. In the presence of HRP, three absorption bands become apparent: a strong band at 421 nm and a broader one with two adsorption maxima at 671 nm and 744 nm. The catalytic reaction was completed after 15 min and a 20 min reaction time was thus chosen before UV/Vis spectra were recorded.[35] The concentration of active HRP linked to the magnetic particles was estimated by recording a calibration curve (Fig. 9B) at 421 nm, characteristic for the formation of the green oxidation product. The calibration curve can be generated by keeping the concentration of ABTS (3.6 mM) and H_2O_2 (50 μM) constant, whereas the amount of HRP injected into the solution is increased step by step. A HRP concentration of 14.6 μg mg^{-1} was determined on MF-MP2, which scales well to HRP found on magnetic particles modified with only dopamine, where 30 μg mg^{-1} HRP was linked.

In a final step, the azide-functions on the magnetic particles reacted with propargylated mannose when mixed together in the presence of $CuSO_4$/L-ascorbic acid as catalyst giving the corresponding mannose-clicked magnetic particles (Fig. 8 reaction 3). The interest in particle linked mannose is based on the current understanding that glycan particles can inhibit bacterial adhesion mediated by type 1 fimbria.[37–39] The loading of linked sugar was estimated using the phenol-sulfuric acid calorimetric method, well-established for analysis of carbohydrates.[40–42] Fig. 9C shows the UV/Vis spectrum of a 1 mL phenol-sulfuric acid solution, where the mannose modified magnetic

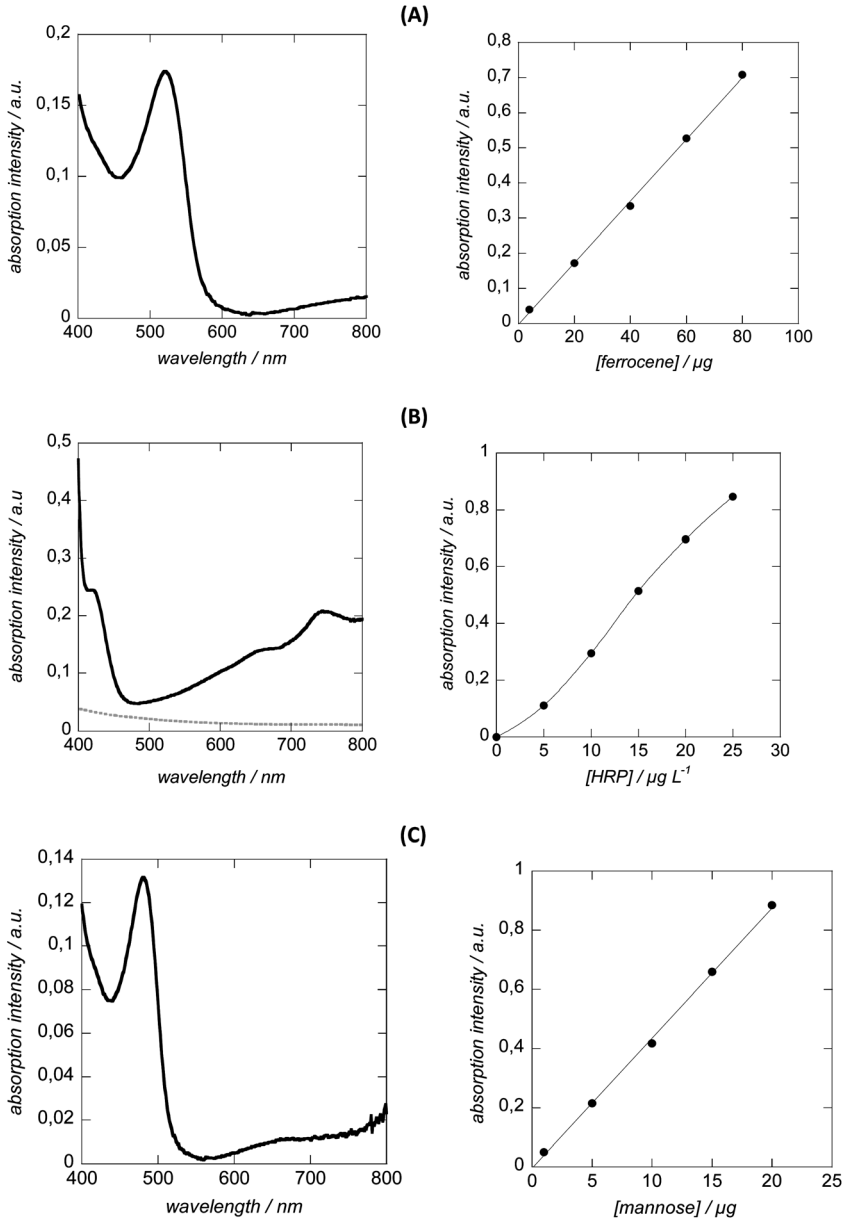

Fig. 9 UV/Vis spectra (left) and calibration curves (right) recorded with subsequently modified MF-MPs: (A) MF-MP1; (B) MF-MP2 (0.5 mg mL^{-1}) in 2 mL of a solution containing ABTS (3.6 mM) and H_2O_2 (50 µM) (black line) and of naked magnetic particles (dotted grey line); (C) MF-MP3 (recorded after 60 min of immersion of 0.2 mg mL^{-1} MF-MP3 in a phenol-sulfuric acid solution).

particles had been immersed for 1 h. By measuring the absorption difference between $\lambda = 570$ nm (baseline) and $\lambda = 481$ nm with reference to a calibration curve a sugar loading of *ca.* 19 µg mg^{-1} was determined. As a comparison, magnetic particles grafted with only dopamine-N_3 gave a clicked mannose loading of *ca.* 60 µg mg^{-1}.

4 Conclusion

We have demonstrated that differently functionalized dopamine derivatives can be separately or simultaneously anchored to Fe_3O_4 nanoparticles by sequential immersion of the particles into a solution of the corresponding dopamine derivatives. These MF-MPs showed comparable magnetic properties to those of naked nanoparticles. As confirmed by TEM and magnetic measurements, the particle size remains almost unaltered with the addition of the different catechol derivatives, indicating *a priori*, monolayer formation. The additional advantage of using dopamine derivatives, besides the protection of the iron oxide shell, is the possibility to integrate in a one-step reaction several reactive sites onto the particles. Here, the reaction with three different dopamine derivatives, carrying amine, azide and maleimide functions, has been used to demonstrate the multi-functionalization principle. However, one might not be limited to the introduction of three surface functions and the concept is easily adaptable to the use of an

increasing number of dopamine derivatives. The conjugation of each of the functional groups separately with model ligands such as thiolated ferrocene, HRP and mannose has been further achieved by performing subsequently, selective covalent binding conditions. As these particles can be designed to exhibit several features synergitically, such MF-MPs are expected to have unique advantages for biomedical applications.

Acknowledgements

Financial support from the Centre National de Recherche Scientifique (CNRS), the Université Lille 1 and the Institut Universitaire de France (IUF) are gratefully acknowledged. Support from the European Union through a FP7-PEOPLE-IRSES (no. 269009) is acknowledged as well as the French Ministry of Foreign Affairs for a doctoral fellowship for M. M. Support from the Romanian project PNII IDEI 75/2011 is gratefully acknowledged.

References

1 J. Gao, H. Gu and B. Xu, *Acc. Chem. Res.*, 2009, **42**, 1097.
2 G. Mistlberger, K. Koran, E. Scheucher, D. Aigner, S. M. Borisov, A. Zankel, P. Polt and I. Klimant, *Adv. Funct. Mater.*, 2010, **20**, 1842.
3 S. Laurent, D. forge, M. Prt, A. Roch, C. Robic, L. Vander Elst and R. N. Muller, *Chem. Rev.*, 2008, **108**, 2064.
4 R. Hao, R. Xing, Z. Xu, Y. Hou, S. Gao and S. Sun, *Adv. Mater.*, 2010, **22**, 2729.
5 N. A. Frey, S. Peng, K. Cheng and S. Sun, *Chem. Soc. Rev.*, 2009, **38**, 2532.
6 C. Tassa, S. Y. Shaw and R. Weissleder, *Acc. Chem. Res.*, 2011, **44**, 842.
7 J. Xie, G. Liu, S. H. Eden, H. Ai and X. Chen, *Acc. Chem. Res.*, 2011, **44**, 883.
8 M. Colombo, S. Carregal-Romero, M. F. Casula, L. Gutiérrez, M. P. Morales, I. B. Bohm, J. T. Heverhagen, D. Prisperi and W. J. Parak, *Chem. Soc. Rev.*, 2012, **41**, 4306.
9 T. D. Schladt, K. Schneider, H. Schild and W. Tremel, *Dalton Trans.*, 2011, **40**, 6315.
10 K. Hayashi, K. Ono, H. Suzuki, M. Sawada, M. Moriya, W. Sakamoto and T. Yogo, *Chem. Mater.*, 2010, **22**, 3768.
11 C. Hui, C. Shen, J. Tian, L. Bao, C. Li, Y. Tian, X. Shi and H.-J. Gao, *Nanoscale*, 2011, **3**, 701.
12 D. Li, W. Y. Teoh, J. J. Gooding, C. Selomulya and R. Amal, *Adv. Funct. Mater.*, 2010, **20**, 1767.
13 C. Xu, K. Xu, H. Gu, R. Zhend, H. Liu, X. Zhang, Z. Guo and B. Xu, *J. Am. Chem. Soc.*, 2004, **126**, 9938.
14 M. Das, D. Bandyopadhyay, D. Mishra, S. Datir, P. Dhak, S. Jain, T. K. Maiti, A. Basak and P. Pramanik, *Bioconjugate Chem.*, 2011, **22**, 1181.
15 R. D. Rutledge, C. L. Warner, J. W. Pittman, R. S. Addleman, M. Engelhard, W. Chouyyok and M. G. Warner, *Langmuir*, 2010, **26**, 12285.
16 A. S. Goldmann, C. Schodel, A. Walther, J. Yuan, K. Loos and A. H. E. Muller, *Macromol. Rapid Commun.*, 2010, **31**, 1608.
17 A. K. L. Yuen, G. A. Hutton, A. F. Masters and T. Maschmeyer, *Dalton Trans.*, 2012, **41**, 2545.
18 B. Roy and B. Mukhopadhyay, *Tetrahedron Lett.*, 2007, **48**, 3783.
19 K. K. Yeoh, T. D. Butters, B. L. Wilkinson and A. J. Fairbanks, *Carbohydr. Res.*, 2009, **344**, 586.
20 M. A. Watson, J. Lyskawa, C. Zobrist, D. Fournier, M. Jimenez, M. Traisnel, L. Gengembre and P. Woisel, *Langmuir*, 2010, **26**, 15920–15924.
21 Y. S. Kang, S. Risbud, J. F. Rabolt and P. Stroeve, *Chem. Mater.*, 1996, **8**, 2209.
22 T. Rajh, L. X. Chen, K. Lukas, T. Liu, M. C. Thurnauer and D. M. Tiede, *J. Phys. Chem. B*, 2002, **106**, 10543.
23 T. Yamashita and P. Hayes, *Appl. Surf. Sci.*, 2008, **254**, 2441.
24 H. Qu, D. Caruntu, H. Liu and C. J. O'Connor, *Langmuir*, 2011, **27**, 2271.
25 A. Barras, J. Lyskawa, S. Szunerits, P. Woisel and R. Boukherroub, *Langmuir*, 2011, **27**, 12451.
26 D. Predoi, V. Kuncser, U. Russo, G. Principi and G. Filoti, *J. Phys.: Condens. Matter*, 2003, **15**, 1797.
27 V. Kuncser, G. Schinteie, B. Sahoo, W. Keune, D. Bica, L. Vekas and G. Filoti, *J. Phys.: Condens. Matter*, 2007, **19**, 016205.
28 C. M. Sorensen, *Nanoscale Materials in Chemistry*, ed. K. J. Klabunde, Johen Wiely and Sons, 2001.
29 M. F. Thomas and C. E. Johnson, *Mossbauer Spectroscopy*, ed. D. P. E. Dickson and F. J. Berry, Cambridge University Press, 1986.
30 N. N. Greenwood and T. C. Gibb, *Mossbauer Spectroscopy*, Chapman and Hall, 1971.
31 R. A. Brand, *Nucl. Instrum. Methods Phys. Res., Sect. B*, 1987, **28**, 398.
32 M. J. Roberts, M. D. Bentley and J. M. Harris, *Adv. Drug Delivery Rev.*, 2002, **54**, 459.
33 C. E. Hoyle and C. N. Bowman, *Angew. Chem., Int. Ed.*, 2010, **49**, 1540.
34 A. D. Baldwin and K. L. Kiick, *Bioconjugate Chem.*, 2011, **22**, 1946.
35 Q. Wang, A. Kromka, J. Houdkova, O. Babchenko, B. Rezek, M. Li, R. Boukherroub and S. Szunerits, *Langmuir*, 2012, **28**, 587.
36 L. Edman, Z. Foldes-Papp, S. Wennmalm and R. Rigler, *Chem. Phys.*, 1999, **247**, 11.
37 C. C. Li, Y. C. Yeh, C. Y. Yang, C. L. Chen, G. F. Chen and C. C. Chen, *J. Am. Chem. Soc.*, 2002, **124**, 3508.
38 A. Barras, F. A. Martin, O. Bande, J.-S. Baumann, J.-M. Ghigo, R. Boukherroub, C. Beloin, A. Siriwardena and S. Szunerits, *Nanoscale*, 2013, DOI: 10.1039/c3nr33826f.
39 A. Roux, C. Beloin and J. M. Ghigo, *J. Bacteriol.*, 2005, **187**, 1001.
40 X. Wang, O. Ramstrom and M. Yan, *J. Mater. Chem.*, 2009, **19**, 8944.
41 M. Durka, K. Buffet, J. Iehl, M. Holler, J.-F. Nierengarten, J. Taganna, J. Bouckaert and S. P. Vincent, *Chem. Commun.*, 2011, **47**, 1321.
42 I. Kaminska, A. Barras, Y. Coffinier, W. Lisowski, J. Niedziolka-Jonsson, P. Woisel, J. Lyskawa, M. Opallo, A. Siriwardena, R. Boukherroub and S. Szunerits, *ACS Appl. Mater. Interfaces*, 2012, **4**, 5386.